Available online at www.sciencedirect.com

SCIENCE DIRECT®

Earth and Planetary Science Letters 234 (2005) 421–435

EPSL

www.elsevier.com/locate/epsl

Microseismicity and creeping faults: Hints from modeling the Hayward fault, California (USA)

R. Malservisi[a,*,1], K.P. Furlong[b], C.R. Gans[b]

[a] *University of Miami, RSMAS, MGG, 4460 Rickenbacker, Cswy, Miami, FL, 33134, USA*
[b] *Geodynamics Research Group, Penn State University, Department of Geosciences, 542 Deike Building, University Park, PA, 16802, USA*

Received 31 August 2004; received in revised form 1 February 2005; accepted 17 February 2005

Editor: S. King

Abstract

Creeping segments of strike-slip faults are often characterized by high rates of microseismicity on or near the fault. This microseismicity releases only a small fraction of the slip occurring on the fault and the majority of the accumulating elastic strain is released either through aseismic creep or in rare large events. Distinguishing between creeping or non-creeping patches on faults and determining the resulting accumulated slip deficit is important in assessing the seismic hazard associated with a fault. Unfortunately, surface creep data alone are insufficient to constrain the creep at depth on the fault. Here we analyze the possibility of using microseismicity as a further constraint. An analysis of the accumulation of Coulomb stress associated with the fault creep indicates that the transition from creeping regions to locked patches has the potential to affect the local seismicity pattern. Precise relative relocations of the microseismicity of the Hayward fault [1] [F. Waldhauser, W.L. Ellsworth, Fault structure and mechanics of the Hayward Fault, California, from double-difference earthquake locations, J. Geophys. Res. 107(3), doi:10.1029/2000JB000084, 2002.] indicate that a fraction of the events repeat, indicating recurrent ruptures of the same small patch. A comparison of the creeping pattern resulting from a Finite Element deformation Model with this precisely relocated microseismicity indicates that the non-repeating earthquakes mainly occur in the transitional zones from creeping to locked patches, while recurrent (repeating) earthquakes cluster in high creep-rate regions. Building from this observation, we have developed an analysis approach to better define patterns of creep, and thus the slip deficit, on the Hayward fault. Additionally this creep rate and its spatial pattern on the fault vary as a function of time after the system is loaded by earthquakes on the locked patches.

Keywords: microseismicity; creeping faults; Coulomb stress; Hayward fault; seismic hazard

1. Introduction

A characteristic of some faults is the accommodation of part of the inter-seismic differential motion

* Corresponding author. Ludwig-Maximilian University, Section of Geophysics, Theresienstr. 41, Munich D-80333, Germany. Tel.: +49 89 2180 4201.
E-mail address: rocco@geophysik.uni-muenchen.de, rmalservisi@rsmas.miami.edu (R. Malservisi).
[1] Tel.: +1 305 361 4928.

0012-821X/$ - see front matter © 2005 Elsevier B.V. All rights reserved.
doi:10.1016/j.epsl.2005.02.039

through fault creep. While most faults and fault segments remain locked between major seismic events, creeping fault segments accommodate some fraction of the motion by slipping essentially aseismically. Creeping faults were first identified along the San Andreas Faults in central California, where cultural features were progressively offset [2]. Apart from the San Andreas fault system in California (which includes the Hayward fault, Fig. 1) [3–5] significant creep at the surface seems to be rare [6] but it has been suggested for segments of faults in strike-slip and trans-compressional regimes [7–10]. On the other hand, creep seems to be quite common at the plate interface in the seismogenic zone in non-fully-coupled subduction zones (e.g. [11,12]). Because most creeping faults appear to release only part of the long-term motion through aseismic slip, they still accumulate a slip deficit; accumulated elastic strain

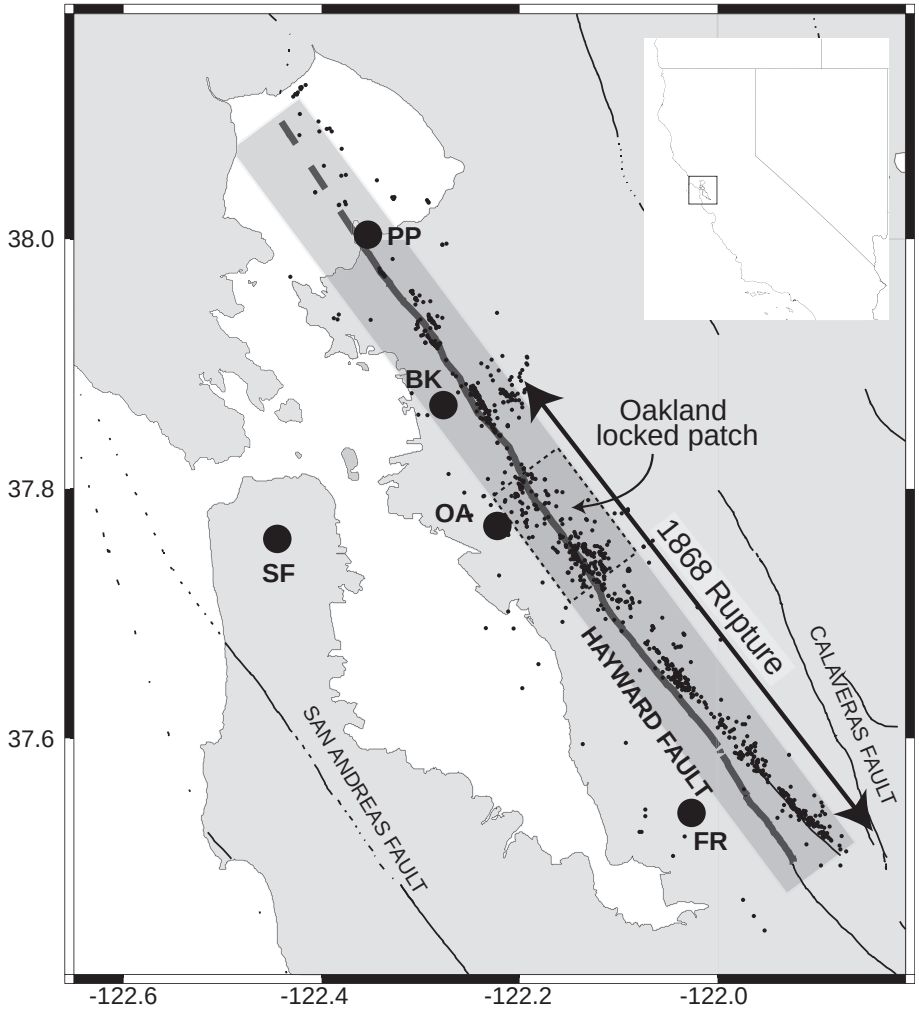

Fig. 1. San Francisco Bay area map with Hayward fault seismicity. The map shows geographical references used in the text and the main faults of the San Andreas fault system [38]. The relocated seismicity from Waldhauser and Ellsworth [1] is indicated by the small solid dots. Our study area in the vicinity of the Hayward fault is highlighted by the gray shaded box; the surface trace of the fault is marked by the thicker line. The double arrow indicates the maximum inferred length of fault rupture during the 1868 earthquake. There is uncertainty about the extent of the 1868 rupture north of Oakland and south of Fremont [24,25]. The insert shows the position of the Bay area with respect to California (PP: Point Pinole, BK: Berkeley, OA Oakland, FR: Fremont, SF: San Francisco).

that is periodically released by medium to large earthquakes. Determining the slip deficit accumulated by a fault is critical for any seismic hazard assessment for the surrounding regions. Unfortunately, models of fault creep constrained only by surface creep observations are highly non-unique and not overly sensitive to the details of the slip behavior at depth, indicating the need for further constraints [13,14].

In general, faults observed to creep also generate significant numbers of small earthquakes on or near the fault [15] and it is common practice to identify creeping segments as those characterized by this on-fault microseismicity [1,15,16]. Although this microseismicity occurs at a high rate, because of its low magnitude range it does not contribute significantly to total fault slip [15,17,18]. The microseismicity associated with creeping faults has been previously inferred to represent small frictionally-locked patches that slide in an unstable way, surrounded by larger regions of stable sliding [1,19–21]. Here, we suggest that this mechanism is responsible only for one part of the microseismicity and that the strain associated with the transition from locked to creeping patches on the fault can generate a large fraction of the microseismicity in the surrounding strained crust. Further we have analyzed the potential for using microseismicity as an aid in constraining the patterns of the creep on the fault by comparing relocated earthquakes with stress, strain, and creep, determined using a 3D Finite Element Model (FEM) that incorporates realistic rheologies.

2. Hayward fault

The Hayward fault (Fig. 1), east of the San Francisco Bay, CA (USA) is a classic example of a creeping fault. Although in some areas the creep at the surface appears to accommodate more than 50% of the long-term displacement [22], the combination

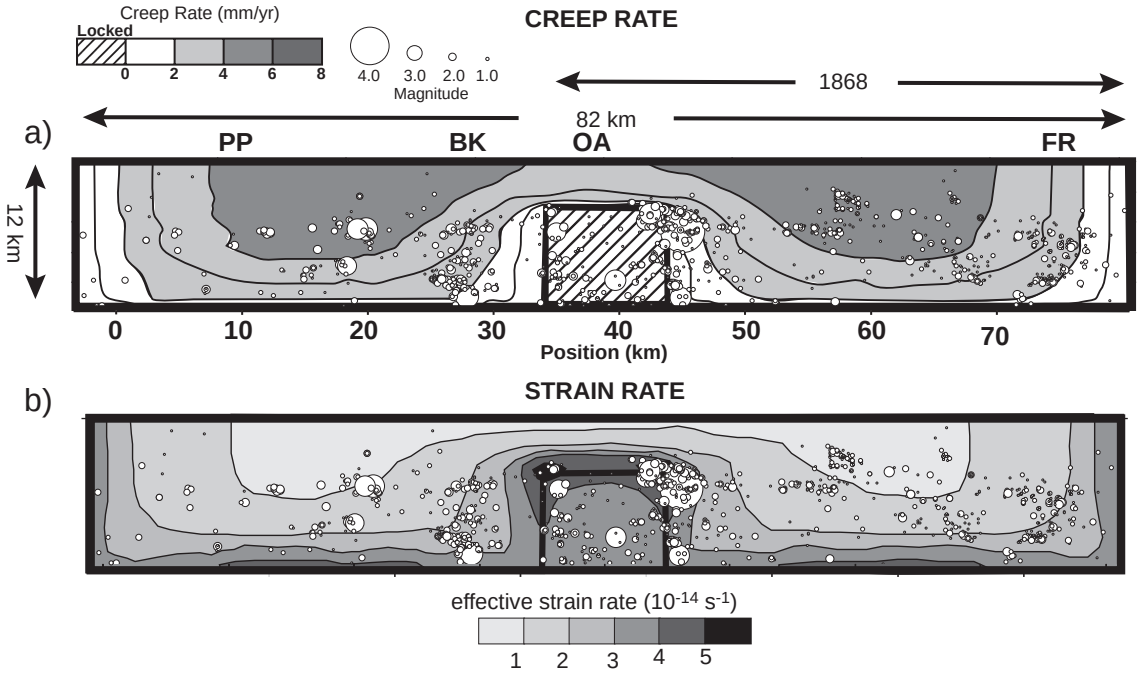

Fig. 2. Fault creep rate and effective strain rate. (a) Fault creep rate for the model 7c-HN from Malservisi [39]. The open circles represent the relocated microseismicity from Waldhauser and Ellsworth [1] (seismicity from 1984 to 1998) projected on the fault plane. As in all following figures, we project seismicity up to 2 km from the fault plane (gray box in Fig. 1). The dimension of the circle is scaled with the event magnitude (magnitude from 0.5 to 3.5). PP, BK, OA and FR as in Fig. 1. The arrow labeled 1868 indicates the estimated maximum extent of the 1868 rupture. (b) Effective strain rate in the crust surrounding the fault (computed 500 m from the fault plane). We use the effective strain rate (defined as $\sqrt{\frac{1}{2}\dot{\varepsilon}_{ij}\dot{\varepsilon}_{ij}}$) as a measure of the magnitude of the strain rate [40]. In this case the effective strain rate is comparable to the shear strain.

of creep plus microseismicity does not account for the long-term slip and the fault does experience moderate to large earthquakes [23,24]. Currently the Hayward fault is listed by the Working Group for California Earthquake Probability (WGCEP) as the highest hazard in the Bay region, although that estimation is also associated with the lowest reliability [22]. The most recent significant event on the Hayward fault is associated with the rupture of the southern segment in 1868 in a magnitude ~6.8 earthquake [23,24]. There is evidence that the last earthquake on the northern segment occurred between 1640 and 1776 AD [23–26].

The pattern of observed surface creep along the Hayward fault [5,27] implies a complexity of creep on the fault plane. Several studies have investigated possible patterns of fault creep on the Hayward fault compatible with surface creep observations [13,17,28–30]. In focusing on the response of a creeping fault to different geometries of locked patches and the interaction of the fault with the surrounding lithosphere, Malservisi et al. [13] showed that creep on the fault plane increases smoothly from locked patches to fully creeping areas (Fig. 2). This transition produces a gradient in creep on the fault plane and thus generates strain in the crust immediately adjacent to the fault. We infer that this strain may be sufficient to generate the diffuse microseismicity on and adjacent to the creeping fault. With this framework, microseismicity can be used to map patterns of creep on faults. The combination of high quality surface creep data [27,29], studies modeling creep and slip deficit [13,14,28–30], and precisely relatively relocated microseismicity [1] allows us to develop a new approach to map patterns of on-fault creep.

3. Hayward fault and microseismicity

Waldhauser and Ellsworth [1] provide precisely relatively relocated events for the Hayward fault. Their seismicity data spans 1984–1998 with magnitudes ranging from 0.5 to 3.5. In spite of the high frequency of events, the total slip produced by the microseismicity is negligible compared to slip occurring through creep [17]. Here we combine the recent study by Waldhauser and Ellsworth [1] of precisely relocated seismicity along the Hayward fault with our 3D model of creep (Model 7c-HN, [13]) to test the hypothesis that deformation in the locked-to-free transition zone generates the observed microseismicity. A comparison of the relocated seismicity with the patterns of creep on the fault and the resulting strain rate in the adjacent crust (Fig. 2) indicates a clustering of events in the transitional areas where the surrounding crust has high strain rate. As indicated above, despite the low friction assigned to those parts of the fault, the regions "shadowed" by the surrounding locked patches have a low creep rate, thus accumulate slip deficit while the surrounding crust is strained. In model 7c-HN, for example, the maximum strain rate occurs in the region surrounding the locked area beneath Oakland (darkest gray in Fig. 2b) and along the border of the creeping section of the fault. Plotting the relocated microseismicity over the strain/creep rate maps (Fig. 2) indicates that it clusters in these high strain rate ($>2\times10^{-14}$ s^{-1}) or equivalently slow creep rate (<22 mm/yr) regions.

We have quantified this correlation between seismicity and creep rates by categorizing the seismicity into creep and/or strain rate bins, computing how much seismicity occurs for each category of creep. As we did in a previous publication [17], the moment associated with each tabulated magnitude was computed using a relation developed by Thatcher and Hanks [31] for Southern California (to convert magnitude to energy) and the relationship from Abercombie [32] (to translate energy to moment). Due to the related uncertainty in correlating the reported magnitude with either seismic moment or energy for the relatively small earthquakes of our study (magnitudes ranging from 0.5 to 3.5), the results are presented both as sum of moment (Table 1) and as sum of magnitude (Table 2). If we exclude the two magnitude 3.5 earthquakes south of the locked region, the conclusions from the two methods are consistent. In the following analysis we discuss only the moment case.

Table 1 summarizes the percentage of cumulative moment released by the earthquakes in the different creep/strain categories with the exclusion of two magnitude 3.5 events. The two bigger events of our catalog were excluded because their moment represents more than 40% of the total moment released by the earthquake in the catalog and would bias the statistics. When compared to model 7c-HN, 54% of the total moment of the relocated earthquakes is

Table 1
Percentage of area and of total moment assigned to different creep-rate categories

Creep rate	7c-HN (Malservisi et al. [13])				KT3 (this paper)			
	% Area	% ∑Moment (all)	% ∑Moment (repeating)	% ∑Moment (non-repeating)	% Area	% ∑Moment (all)	% ∑Moment (repeating)	% ∑Moment (non-repeating)
Locked	101	29.5	9.1	34.5	11	31.9	9.7	39.3
0–2 mm/yr	21	24.6	1.7	30.8	25	12.2	0.7	13.7
2–4 mm/yr	40	17.6	3.3	22.4	41	38.2	2.0	39.2
4–6 mm/yr	29	28.3	85.9	12.3	23	17.8	87.6	7.8

% ∑Moment (all): percentage of cumulative magnitude released by all the relocated events.
% ∑Moment (repeating): percentage of cumulative magnitude released by the events within a radius of 150 m from the events defined as repeating by Waldhauser and Ellsworth [1].
% ∑Moment (non-repeating): percentage of the cumulative magnitude released by the relocated events not identified as repeating and not within 150 m of repeating earthquakes.

released in the region creeping less than 2 mm/yr (strain rate $>1.5\times10^{-14}$ s^{-1}), a region that corresponds to only 31% of the fault area. In contrast, 28% of the seismicity is released in the fully creeping region (rate >4 mm/yr) which corresponds to ~29% of the area. A close analysis of Fig. 2 also shows that many of the events assigned to the locked patches are located close to the edge of those patches. Incidentally we want to note that the two relatively bigger earthquakes happen in this transitional area as well; if we include those events, 93% of the moment is released in regions creeping less than 2 mm/yr. This observation is in agreement with the results of Tse et al. [33], who found that stress concentrates at the border of locked patches.

In their study, Waldhauser and Ellsworth [1] identified a subset of earthquakes that appear to be repeated ruptures of the same small asperities (solid circles in Fig. 3a). They referred to this subset as repeating or recurring earthquakes. It has been argued that such repeating earthquakes represent very small locked patches surrounded by free-slipping regions of the fault [19–21]. Taking into account the rupture size [17], the resolution in the relocations of the event, the fact that some of the repeated events are not exactly co-located (e.g. Fig. 10 of Waldhauser and Ellsworth [1]), and the incompleteness of the catalog of recurrent events, we consider here as recurrent all the events falling within 150 m of events identified as repeating by Waldhauser and Ellsworth [1]. More than 80% of the summed moment released by repeated earthquakes is in the fully-creeping area, consistent with the model of these events representing small locked patches (mini-asperities) within a free-slip region. When we remove the repeating earthquakes from the data set and repeat the analysis of comparing cumulative moment with creep rate, we find that earthquakes in the fully-creeping region (creep rate >4 mm/yr, 29% of area) release only 12% of the total moment while earthquakes in the high-strain region

Table 2
Percentage of area and of total magnitude assigned to different creep-rate categories

Creep rate	7c-HN (Malservisi et al. [13])				KT3 (this paper)			
	% Area	% ∑Magnitude (all)	% ∑Magnitude (repeating)	% ∑Magnitude (non-repeating)	% Area	% ∑Magnitude (all)	% ∑Magnitude (repeating)	% ∑Magnitude (non-repeating)
Locked	10	17.4	10.6	18.8	11	18.5	11.4	19.3
0–2 mm/yr	21	26.3	17.8	28.1	25	29.7	18.8	30.9
2–4 mm/yr	40	37.8	5.3	44.3	41	38.2	18.9	46.1
4–6 mm/yr	29	18.5	66.3	8.8	23	17.8	50.9	3.6

% ∑Moment (all): percentage of cumulative magnitude released by all the relocated events.
% ∑Moment (repeating): percentage of cumulative magnitude released by the events within in a radius of 150 m from the events defined as repeating by Waldhauser and Ellsworth [1].
% ∑Moment (non-repeating): percentage of the cumulative magnitude released by the relocated events not identified as repeating and not within 150 m of repeating earthquakes.

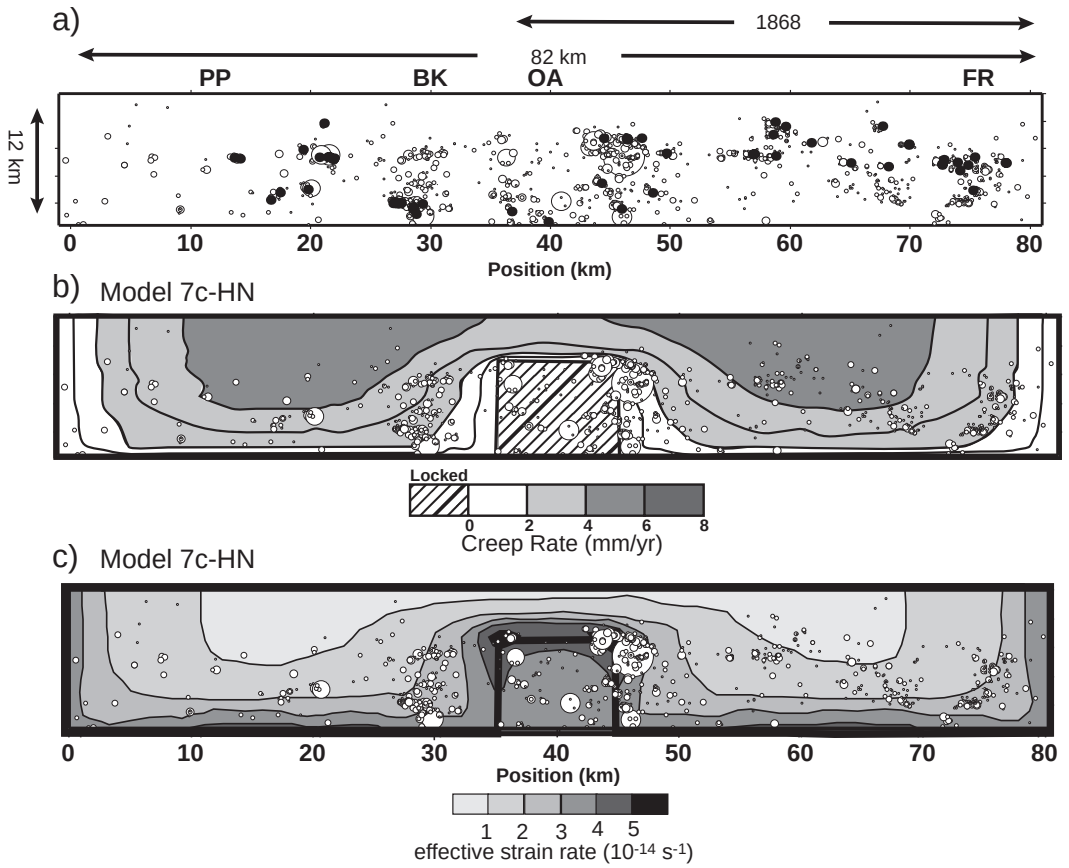

Fig. 3. Comparison between non-recurrent earthquakes and model 7c-HN results. (a) Relocated microseismicity along the Hayward fault (open circles) adapted from [1]. The circles are scaled according to their magnitude (see Fig. 2). The solid circles represent clusters of earthquakes defined as recurrent by Waldhauser and Ellsworth [1]. In the analysis, we also considered as recurring all the earthquakes within 150 m of these events. (b) Comparison of fault creep as evaluated in Fig. 2 and non-recurrent seismicity. (c) Comparison between off-fault strain rate from the model 7c-HN and the non-recurrent microseismicity.

(creep rate <2 mm/yr; 31% of area) release ~65% (Table 1, Fig. 3).

4. Locked patches and Coulomb stress

A locked patch represents a region on the fault plane allowing no differential motion across the fault, except during an earthquake. However, because the crust surrounding the fault is a continuum, there cannot be step discontinuities in displacement (except across the fault itself). As a result, there is a transitional region from the fully-locked to the free-slip region of the fault. Although the fault properties in the transitional area allow free slip, the proximity to the locked patch reduces the slip on the fault. These locked and transitional regions slide at a velocity slower than the surrounding creeping regions and thus accumulate strain energy within the crust adjacent to the fault at a faster rate.

To test the potential influence of the interaction between creeping and locked patches on the local stress field, and thus on the microseismicity, we analyze the Coulomb stress associated with the modeled pattern of creep. For this analysis we use a simplified approach, using Coulomb 2.5 [34] to determine the rate of Coulomb stress developed. This simple 3D elastic modeling allows us to focus on the role of locked and free patches within the elastic upper crust in generating a distribution of Coulomb

stress (and seismicity). Similar results are obtained using more complete 3D viscoelastic modeling. With such modeling, however, it is difficult to isolate the effects of the fault patterns from the overall effects of viscous localization and relaxation in the lower crust. Using the code Coulomb 2.5, we calculate the yearly stress changes in an elastic half-space due to creep on the Hayward fault, derived by model results of Malservisi et al. [13], assuming steady-state creep. The absolute value of the Coulomb stress is also dependent on the regional stress field, an uncertain parameter. For consistency with our FEM boundary

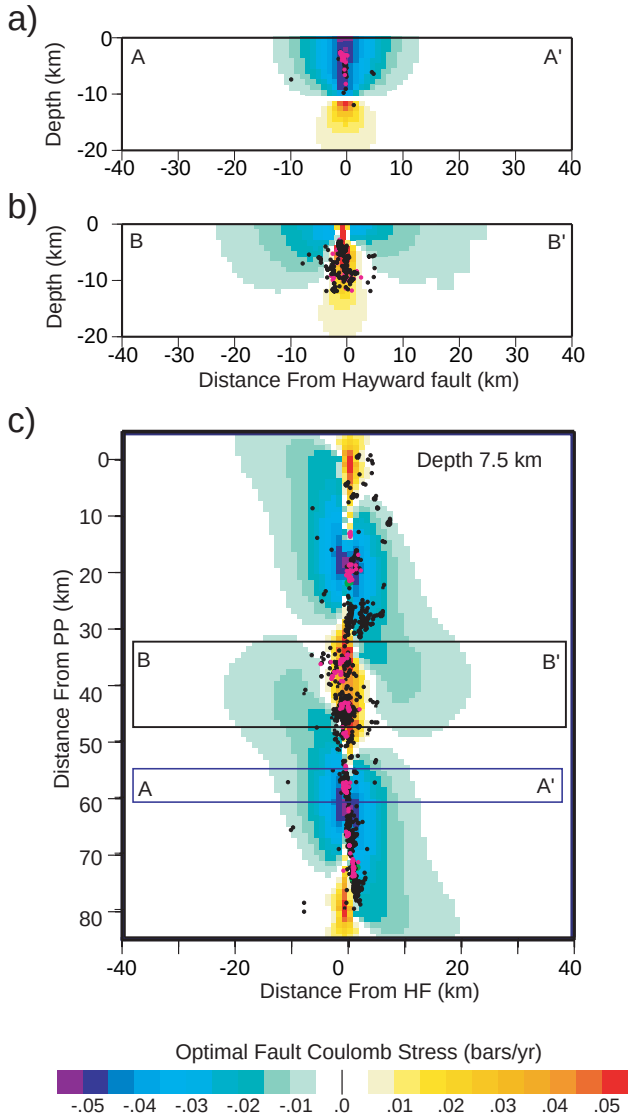

Fig. 4. Results from Coulomb stress computation compared with relocated seismicity. (a) Vertical cross section in a rapidly creeping region (position ~60 km). Note that the Coulomb stress is low, the seismicity is localized on the fault, and the majority of the seismicity is represented by repeating events (magenta dots). (b) Vertical cross section in the region beneath Oakland (locked patch). Note the high Coulomb stress, seismicity diffuse over a large area (~corresponding to the area of high Coulomb stress) and prevalence of non-repeating events (black dots). (c) Horizontal slice at 7.5 km depth (through the middle of the locked patch beneath Oakland). Boxes represent the areas where the seismicity has been projected for the vertical cross sections (a and b).

conditions we assume that regional stress is given by a simple shear stress parallel to the fault of 6 kPa/yr, a stress compatible with previous calculations [35,36].

Fig. 4 shows the results from the Coulomb stress calculation for the best-oriented strike-slip fault compared with the relocated microseismicity. The top two panels correspond to two vertical slices located in the rapidly creeping region in the south (a) and in the locked region of Oakland (b). The lowest panel shows a horizontal slice at 7.5 km depth (at this depth the patch beneath Oakland is locked). There are several important features of the stress field:

(1) there is negative Coulomb stress corresponding to the rapidly creeping regions. This is compatible with the fact that creep is releasing part of the elastic strain accumulating at the plate boundary. The negative Coulomb stress should map a reduction in the microseismicity in the surrounding lithosphere. It is interesting to note that in the low (negative) Coulomb stress region the microseismicity is mostly aligned with the fault and the repeated earthquakes (magenta dots) represent the majority of the activity.

(2) In the transition zone and in the area surrounding the locked patch, the Coulomb stress is positive. In particular we can see that the high (positive) Coulomb stress region (the region where the stress regime is more favorable for the seismicity) is a broad region adjacent to the fault plane. It is interesting to note that the relocated microseismicity in this area is not aligned with the fault plane but rather tends to

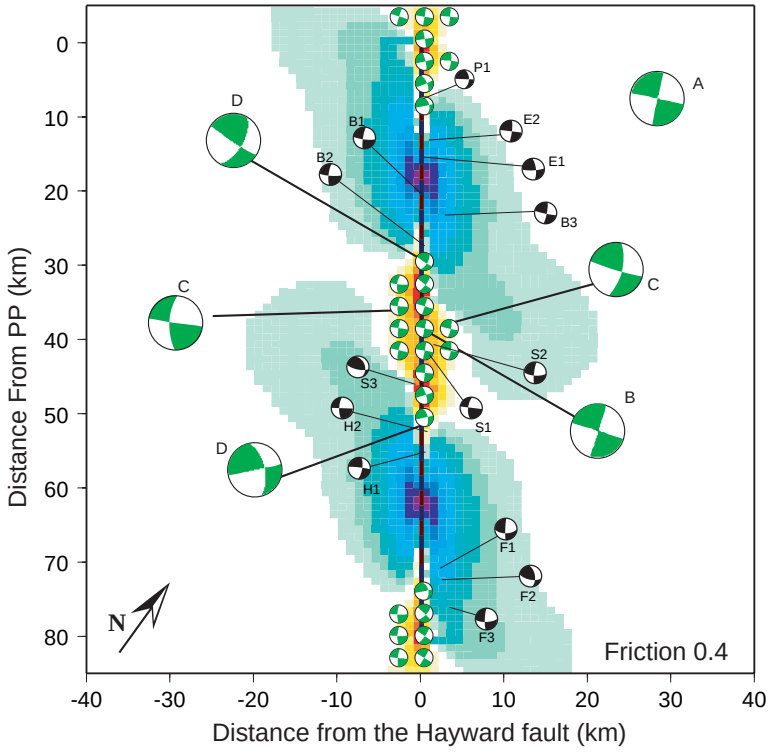

Fig. 5. Focal mechanisms for the optimally-oriented fault computed using Coulomb 2.5 [34], a friction coefficient of 0.4, and regional shear stress from numerical models [13,35,36]. We plot only the right-lateral mechanisms; similar rotations are present for left-lateral ones. Only the mechanisms in regions of positive Coulomb stress (for strike-slip fault) have been plotted. We enlarge example mechanisms representing important features (see text for analysis). (A) Regional stress optimally-oriented rupture. (B) Focal mechanisms on the fault plane inside the locked patch. (C) Mechanisms on the crust surrounding the locked patch. (D) Mechanisms at the top of the locked patch. The black mechanisms correspond to the composite focal mechanisms observed by Waldhauser and Ellsworth [1] rotated in the fault parallel reference frame of the figure. The labels correspond to their naming scheme. Coulomb stress plotted using the same color scale of Fig. 4.

cluster in a broader region roughly the size of the positive Coulomb stress area.

(3) The change in Coulomb stress in the transition from locked to fully-creepable regions also should rotate focal mechanisms. Fig. 5 shows model-determined focal mechanisms at 7 km depth oriented in the direction of the maximum Coulomb stress (the most favorable direction of slip during a seismic event). For simplicity we have plotted focal mechanisms only in the region corresponding to positive Coulomb stress. The focal mechanisms are highly sensitive to the regional stress and the friction angle; nevertheless we note a consistent pattern in all our models. Mechanisms located on the fault plane but within the locked patch (B in Fig. 5) are similar to mechanisms that would be produced by the regional stress field. In the crust to the side of the locked patch (C) the mechanisms show a change in dip of the rupture plane. The highest rotation is observed at the tip of the locked patch (D). Note that although these results cannot be considered conclusive due to their sensitivity to the regional stress field, almost all the composite focal mechanisms from Waldhauser and Ellsworth [1] (with the exception of S3) have a similar rotation to the ones computed.

5. Using seismicity to map the fault creep

As discussed above, the transition from a large locked patch to a fully creepable fault alters the stress field and thus can influence the amount, distribution, and the type of seismicity. In particular, we can place additional constraints on patterns of locked patches and fault creep by using the observation that the "normal" microseismicity clusters in the transition areas while the repeated seismicity is more prevalent in highly creeping regions. For example, we can add small locked patches in areas where non-repeated earthquakes cluster. The region around position 60 km (Fig. 3) is a good candidate to test this hypothesis. Although model 7c-HN indicates that this region is fully creeping, the area produces a significant amount of non-repeating earthquakes, suggesting the presence of a locked patch. As shown by Malservisi et al. [13], the

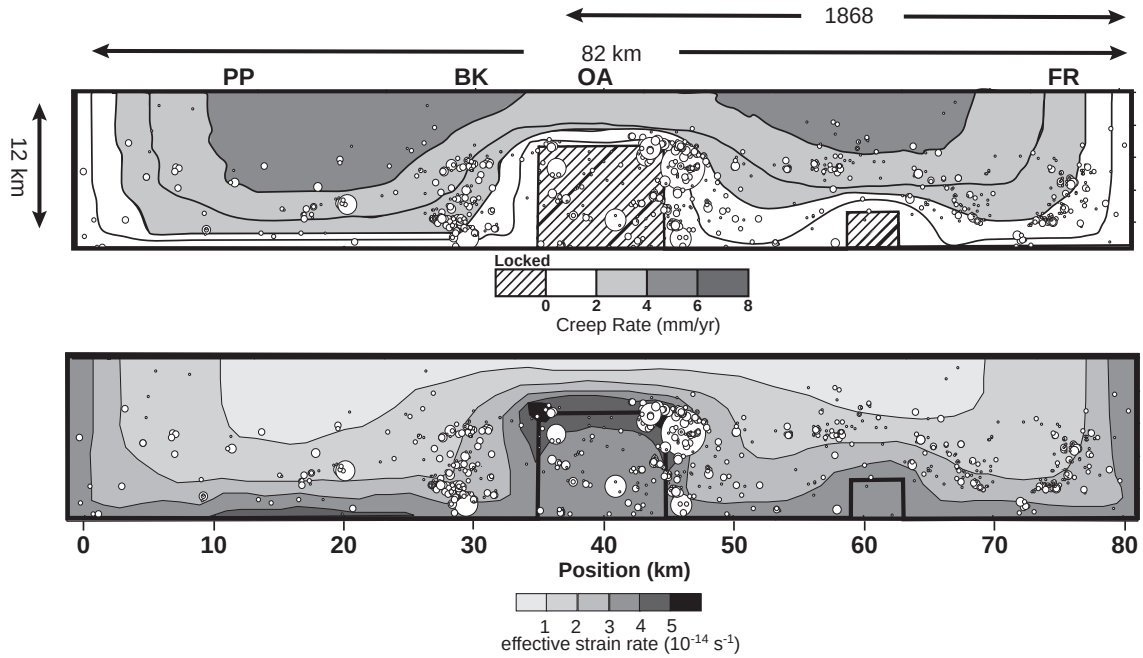

Fig. 6. Fault creep and strain rate for the model with two locked patches (KT3). The locked patch in the southern segment has been added in order to reduce the percentage of non-recurrent seismicity in the fully-creeping region.

surface creep is not highly sensitive to the presence of deep and/or small locked patches. The addition of the patch in position 60 km (Fig. 6) modifies the surface creep rate within the observed errors (Fig. 7). The new classification of the seismic moment released according to creep rate category is reported in Tables 1 and 2. The addition of the locked patch decreases the percentage of moment released by the non-repeated earthquakes in the fully creeping region from 12% to 7%. At the same time, the addition of the locked patch changes the surface creep pattern only within the observed errors (Fig. 7). Fig. 6 show that, as expected, the distribution of the non-repeated earthquakes of model KT3 closely follows the strain rate pattern of the crust surrounding the fault plane.

With repeated iterations of this process we can potentially further improve the correlation between type of seismicity and creep rate. We could for example add a locked patch near the deep events at position 20 km and the Berkeley region, or we could reduce the spatial extent and/or modify the shape of locked patches (e.g. the cluster of non-repeating earthquakes suggests that the locked patch beneath Oakland is not really a simple box shape but may extend at depth further north). Unfortunately, the current resolution of our model (the effect of locked patches smaller than ~5 km^2 cannot be analyzed) does not allow a further refinement. Since this is a first attempt to use the microseismicity to help constrain locked/creeping patches on the fault, we have not extended the application to such fine spatial resolution.

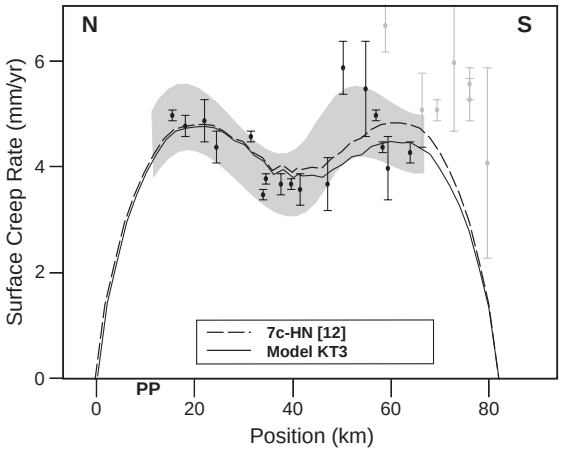

Fig. 7. Comparison between observed geodetic data (adapted from Lienkaemper et al. [27]) and the results of our models. The shaded area represents the best-fit for long-term surface creep rate along the Hayward fault. Both the surface creep rate computed by Malservisi [39] (model 7c-HN, dashed line) and the modified model that uses seismicity as a further constraint (KT3 this paper, continuous line) fit the observed data (shaded area). As with all previous models, we do not account for the high creep rate at the southern end of the fault (gray data points), which appear to be a result of interactions with the surrounding faults. The Hayward fault goes offshore at Point Pinole (PP in Fig. 1, position 12 km). For this reason, the creep rate in the northernmost area (0–12 km) is not constrained.

6. Discussion

Observations of surface creep rate are not sufficient to unequivocally determine the pattern of creep on the fault, particularly at depth. Precise locations for the microseismicity along creeping faults are potential tools to better constrain the pattern of locked and creeping patches on the faults themselves. Another approach for improving resolution at depth is to use the surface strain field in the region surrounding the fault and not merely on-fault creepmeters. In principle, the use of off-axis data should be somewhat more sensitive to the deep behavior of the fault and the use of such a data set should slightly improve the calculation of slip at depth. Unfortunately, the areas most sensitive to the behavior of the Hayward fault at depth are offshore in the San Francisco Bay area to the west or in the steep hilly area to the east, both regions not particularly suitable to geodetic measurements. The Active Tectonics group at the University of California Berkeley is currently analyzing the available data from the San Francisco Bay area GPS network (BARD network) and InSar data [14,37]. Their results show a fault creep pattern similar to the one we obtained using the microseismicity (KT3) but in spite of the additional constraints from off-fault data the creep behavior at depth is still non-uniquely determined.

Recurrent seismicity, where earthquakes appear to be repeated ruptures of the same small asperities, predominantly occurs within the fully creeping regions, while the non-recurrent seismicity clusters in the transitional creeping zones, regions of high strain rate. With this assumption/observation, we can refine the pattern of fault creep, as shown by the above method used to obtain model KT3 for the Hayward fault.

It is important to note that the transition from locked to creeping patches is not limited to strike-slip faults. It also appears to be a fundamental component in the behavior of the seismogenic zone in non-fully-coupled subduction regions, where one commonly speaks of the transition from completely locked to partially locked (or free slipping) while doing an evaluation of the plate coupling. Mapping the location of the locked patches is a critical part of hazard analysis in subduction zones. Because strain is mainly accumulating in these areas, they become the sites of dominant moment release. The study of Norabuena et al. [11] is an example of such behavior. A comparison of the map of slip on the fault plane obtained by inverting geodetic observations in the Costa Rica region with the microseismicity recorded by a local array shows a similar pattern to the one we observed, with the events clustering in the areas surrounding strongly-coupled patches.

6.1. Moment accumulated by a creeping fault

In general, if one assumes a steady-state behavior for a creeping fault, it becomes possible to estimate the slip deficit accumulated by the fault and thus to further constrain the hazard. As an example, we can estimate the slip deficit on the Hayward fault, as generated by creep rate obtained using model KT3, assuming that the present motion represents the long-term fault slip rate and that the computed creep rate can be extrapolated over time. Fig. 8a shows the resulting slip deficit averaged over the seismogenic thickness for the 9 mm/yr long-term (i.e. geologic) slip rate estimated for the Hayward fault [28,29,33]. Poorly-constrained boundary conditions at the north end of the model (position 0–10 km, where the fault is offshore) and fault complexity at the southern end (position >70 km, where the Hayward interacts with a complex network of faults) preclude placing significance on the slip deficit predicted by our models in those regions. On the central part of the fault (position ~40–60 km), the model produces a vertically-averaged slip-deficit accumulation of ~6.5 mm/yr. The accumulated deficit increases around the locked patch beneath the Oakland region (>7.5 mm/yr). On the northern segment (position 10–30 km), the model predicts 5 to 6 mm/yr of slip deficit accumulation. Integrating over the earthquake cycle it is possible to estimate the total slip deficit accumulated and thus the amounts of moment (elastic energy) storage on the fault. Fig. 8b shows the deficit accumulated in a 350 yr period (a time compatible with the recurrence interval on the Hayward fault [23,24] and approximately the time since the 17th century event). On the southern segment (position ~50–60 km), the model generates a slip-deficit accumulation of ~2.5 m over the period. Subtracting the assumed slip of ~1.9 m during the 1868 event [25] the net deficit would be on the order of ~0.6 m. Since the northern limit of the 1868 rupture is not well constrained, the slip deficit in the Oakland region is difficult to quantify. The large locked patch will generate the highest slip deficit (on the order of 3 m) but it is possible that the 1868 event released a large part of this accumulated moment (in Fig. 9b we assume that this area was affected by the 1868 event [25]). On the northern segment (position ~10–30 km) our model produces a slip deficit of ~2 m. The absence of rupture during the 1868 event marks this region as having the highest present day accumulated slip deficit.

6.2. Time dependent creep rate

While the pattern of creep on the fault plays a primary role in the accumulation of slip deficit, the additional effects of the earthquake cycle, including the1868 earthquake and previous earthquakes, also affects the pattern of the net accumulated seismic moment on the fault. An additional consideration when evaluating the pattern of accumulated slip deficit is the possibility for transient creep behavior throughout the earthquake cycle. In determining slip deficit through a comparison of the long-term slip rate with the present pattern of fault creep, we have implicitly assumed that the creep rate and the pattern we have found for the present is constant over time. It is reasonable, however, that large events such as the 1868 earthquake in the southern segment, or a possible 17th century event for the northern segment, could have large transient effects on fault creep.

A simple example of this potential post-earthquake transient effect on creep rate is given in Fig. 9. The simulation shows the evolution of the creep over the fault plane of model 7c-HN after an imposed differential slip of 1 m (corresponding to a magnitude ~6.1 earthquake) on the locked patch beneath Oakland. The

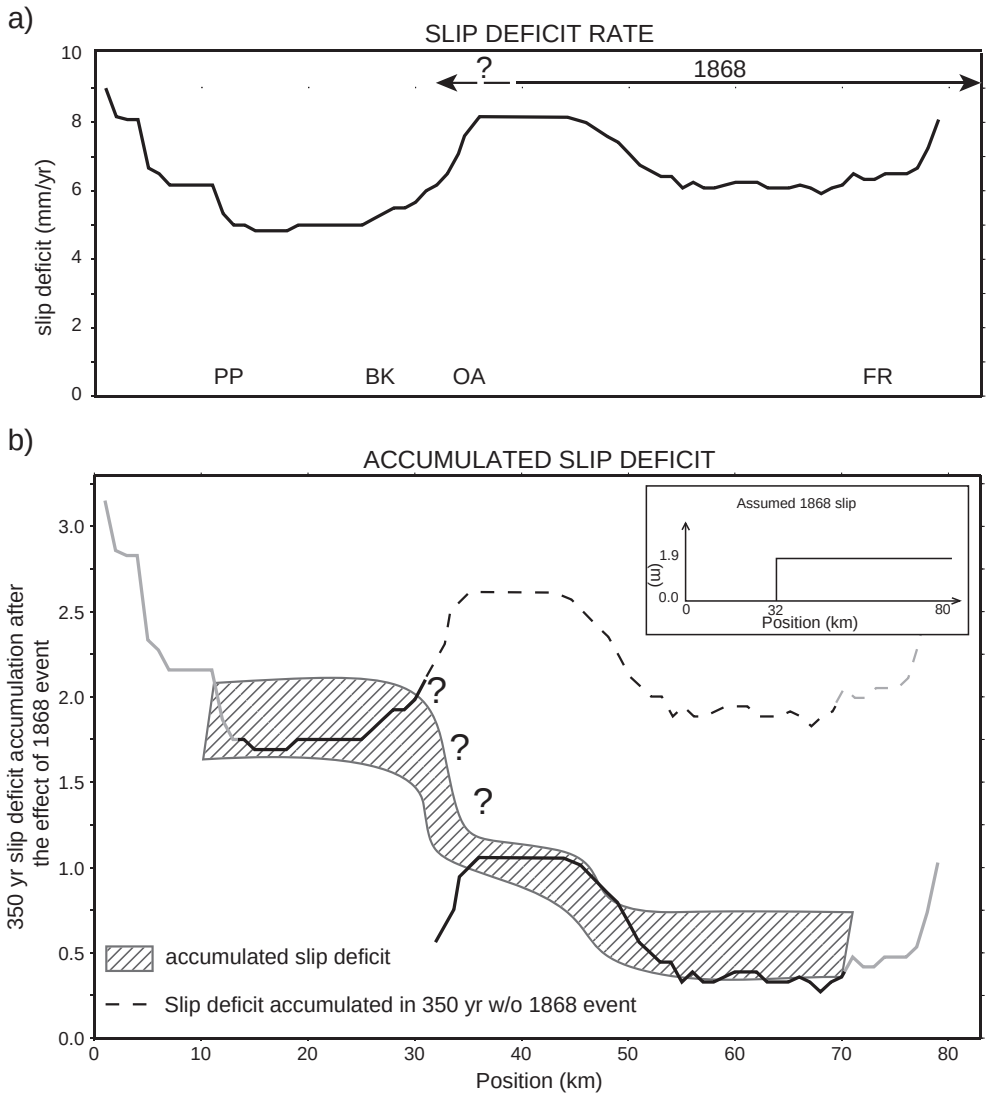

Fig. 8. Hayward fault slip deficit. (a) Vertically-averaged slip deficit rate in the seismogenic layer predicted by model KT3 assuming a 9 mm/yr long-term slip rate on the Hayward fault. The double-arrowed line indicates the extent of the 1868 rupture [21]. (b) Slip deficit accumulated on the seismogenic layer during the past 350 yr assuming a constant slip deficit rate as in Fig. 9a (continuous line on the northern side, dashed line for the area affected by 1868 earthquake). For the 350 yr average we subtract the slip released in the 1868 event (1.9 m, inset) from the slip deficit accumulated in the southern segment of the fault (position >32 km). The slip deficit in the transition from the northern and the southern segment is dependent on the poorly-constrained extent and coseismic slip of the 1868 earthquake (question marks). The shaded area schematically shows average slip deficit inferred from the model results. The northern (position 0–13 km) and the southern (position 70–82 km) ends of the model are not interpreted because the surface creep data are poorly constrained or influenced by the interaction of the surrounding faults.

fault displacement and the stress released by the earthquake alter the flow in the viscoelastic layer, inducing faster flow beneath the fault. This faster flow increases the load on the creeping sections and thus the creeping rate on the fault plane. These effects decay exponentially to the steady-state regime over a time that depends on the local viscosity and fault rupture geometry. It is interesting to note in the

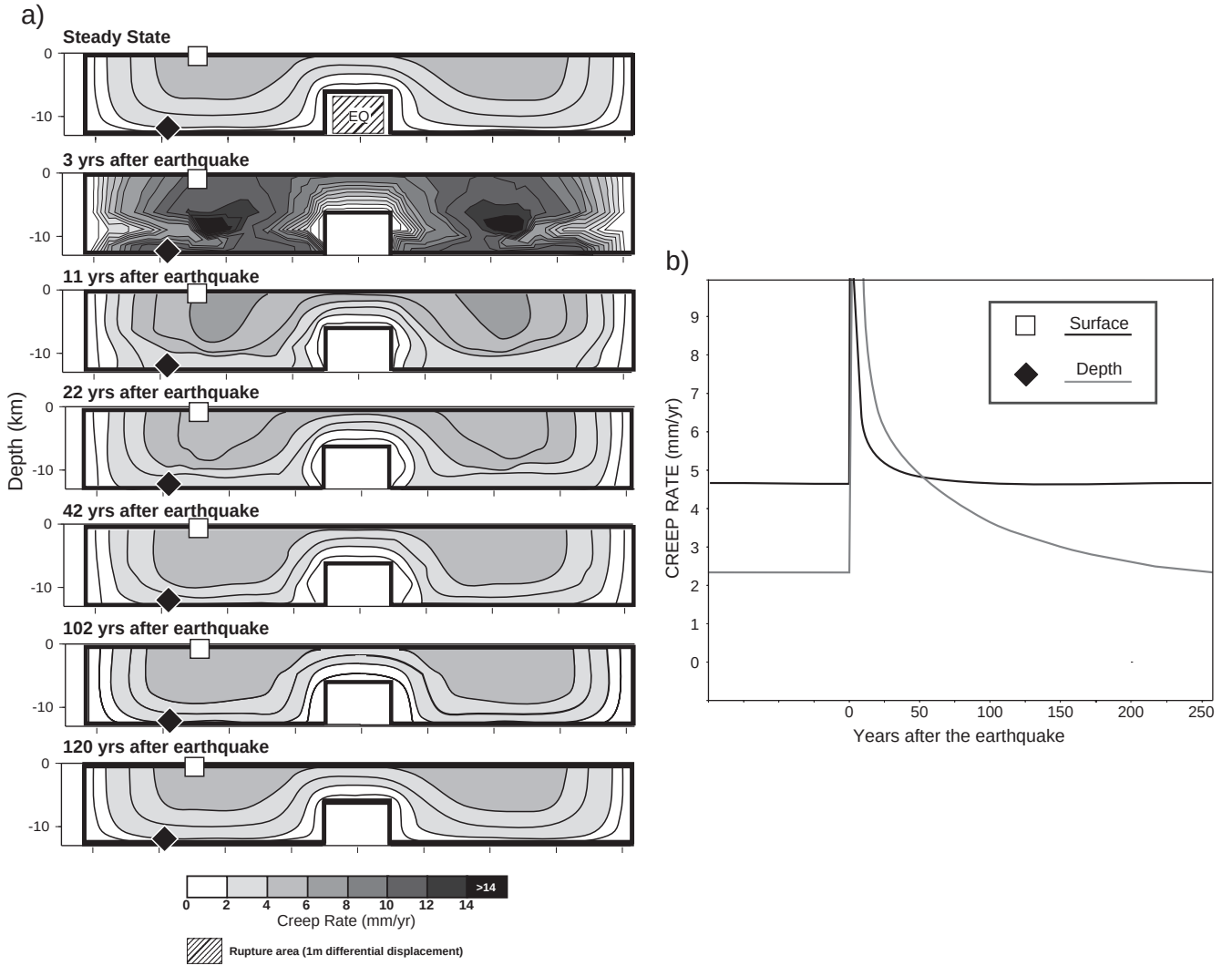

Fig. 9. Transient creep rate on the fault plane after a seismic event on the locked section beneath Oakland. (a) Creep rate on the fault at different times after 1 m of differential displacement is imposed in the dashed area (steady-state figure). The differential displacement is imposed using the split nodes method [41]. Note the high influence on the creep rate at depth. The two symbols in creep rate panel correspond to the two points where we computed the creep rate plot in b. (b) Simulation of the creep rate history for the two depths indicated in a after the 1 m displacement seismic event in the locked area beneath Oakland.

example shown here that the characteristic recovery time is faster for shallow than for deep regions of the fault, indicating the possibility that even when observations at the surface indicate a return to the steady-state regime, deep regions of the fault can still be affected by the transient creep. The use of steady-state assumption for the slip deficit estimation will lead to an overestimation of total accumulated slip deficit. For these reasons, knowing the extent of the rupture and the amount of slip during the events is crucial for estimating the current pattern of stored elastic energy accumulated on the fault. Unfortunately, neither rupture extent nor slip are well-constrained for the 1868 event and virtually unconstrained for the 17th century event. These uncertainties complicate attempts at risk assessment for the region.

The location of the northern termination of the 1868 rupture and the likely decrease in slip magnitude near that terminus also affects the earthquake cycle scenario for the fault. A shorter rupture than the one used in our analysis or a smaller coseismic slip in the Oakland area (position ~30–50 km) would leave a large slip-deficit accumulation in that locked patch. Depending on the different 1868 rupture scenarios, this deficit would have been released to different amounts, leaving significantly different risk residuals. It is interesting to note that the Oakland region appears to have been involved in both the 1868 event of the southern segment and the 17th century event of the northern (?) segment [24]. This locked patch accumulates slip deficit faster than the surrounding areas. Furthermore, the transition from this large locked patch to freely-creeping regions induces a large strain and stress localization at its boundary. Tse et al. [33] suggested that these regions of higher stress are responsible for the nucleation of large ruptures, thus the Oakland locked patch may play some role in the rupture initiation or the termination of large events on the Hayward fault.

Acknowledgements

We thank R. Bürgmann, S. Cohen, A. Rubin and an anonymous reviewer for the thorough reviews and the comments and suggestions that greatly improved the paper. We are also grateful to C. Ammon, R. Engel, D. Fisher, and A. Nyblade for their internal reviews. RM has been supported by several NASA grants awarded to T.H. Dixon. CRG was supported under an NSF Graduate Research Fellowship. This research has been partially supported by the NEHRP Grant 04HQGR0040.

References

[1] F. Waldhauser, W.L. Ellsworth, Fault structure and mechanics of the Hayward Fault, California, from double-difference earthquake locations, J. Geophys. Res. 107 (3) (2002), doi:10.1029/2000JB000084.
[2] K.V. Steinbrugge, E.G. Zacher, D. Tocher, C.A. Whitten, C.N. Claire, Creep on the San Andreas fault, Bull. Seismol. Soc. Am. 65 (1960) 93–112.
[3] J.J. Lienkaemper, G. Borchardt, M. Lisowski, Historic creep rate and potential for seismic slip along the Hayward fault, California, J. Geophys. Res. 96 (B11) (1991) 18261–18283.
[4] J.J. Lienkaemper, J.S. Galehouse, New evidence doubles the seismic potential of the Hayward fault, Seismol. Res. Lett. 69 (6) (1998) 519–523.
[5] J.S. Galehouse, J.J. Lienkaemper, Inferences drawn from two decades of alinement array measurements of creep on faults in the San Francisco Bay Region, Bull. Seismol. Soc. Am. 93 (6) (2003) 2415–2433.
[6] C.H. Scholz, Mechanics of faulting, Annu. Rev. Earth Planet. Sci. 17 (1989) 309–334.
[7] N.N. Ambraseys, Some characteristic features of the Anatolian fault 20 zone, Tectonophysics 9 (2–3) (1970) 143–165.
[8] A. Aytun, Creep measurements in the Ismetpasa region of the North Anatolian fault zone, in: A.M. Isikara, A. Vogel (Eds.), F. Vieweg, Wiesbaden, 1982.
[9] A.G. Sylvester, Strike-slip faults, Geol. Soc. Amer. Bull. 100 (11) (1988) 1666–1703.
[10] J. Lee, J. Angelier, H.T. Chu, J.C. Hu, F.S. Jeng, R.J. Rau, Active fault creep variations at Chihshang, Taiwan, revealed by creepmeter monitoring, 1998–2001, J. Geophys. Res. 108 (B11) (2003), doi:10.1029/20035B002394.
[11] E. Norabuena, T.H. Dixon, S. Schwartz, H. DeShon, M. Protti, L. Dorman, E.R. Flueh, V. Gonzales, P. Lundgren, A. Newman, F. Pollitz, D. Sampson, Geodetic and seismic constraints on some seismogenic zone processes in Costa Rica, J. Geophys. Res. 109 (B11) (2004), doi:10.1029/2003JB002931.
[12] H. Dragert, K. Wang, T.S. James, A silent slip event on the deeper Cascadia subduction interface, Science 292 (5521) (2001) 1525–1528.
[13] R. Malservisi, C. Gans, K.P. Furlong, Numerical modeling of strike-slip creeping faults and implications for the Hayward fault, California, Tectonophysics 361 (1–2) (2003) 121–137.
[14] D. Schmidt, R. Bürgmann, R.M. Nadeau and M. d'Alessio, Distribution of aseismic slip-rate on the Hayward fault inferred from seismic and geodetic data, J. Geophys. Res. (submitted for publication).

[15] C.H. Scholz, The Mechanics of Earthquakes and Faulting, Cambridge Univ. Press, Cambridge, Cambridge, UK, 1990, 413 pp.
[16] A.M. Rubin, D. Gillard, J.L. Got, Streaks of microearthquakes along creeping faults, Nature 400 (6745) (1999) 635–641.
[17] C.R. Gans, K.P. Furlong, R. Malservisi, Fault creep and microseismicity on the Hayward fault, California: implications for asperity size, Geophys. Res. Lett. 30 (19) (2003), doi:10.1029/20036L017904.
[18] F. Amelung, G. King, Earthquake scaling laws for creeping and non-creeping faults, Geophys. Res. Lett. 24 (5) (1997) 507.
[19] J.E. Vidale, W.L. Ellsworth, A. Cole, C. Marone, Variations in rupture process with recurrence interval in a repeated small earthquake, Nature 368 (6472) (1994) 624–626.
[20] R.M. Nadeau, W. Foxall, T.V. McEvilly, Clustering and periodic recurrence of microearthquakes on the San Andreas Fault at Parkfield, California, Science 267 (5197) (1995) 503–507.
[21] C.G. Sammis, J.R. Rice, Repeating earthquakes as low-stress-drop events at a border between locked and creeping fault patches, Bull. Seismol. Soc. Am. 91 (3) (2001) 532–537.
[22] W.G.C.E. Probabilities, Earthquake Probabilities in the San Francisco Bay region: 2003-203 1. Open-File Reptort, OFO3-214, U.S. Geological Survey, Reston, VA, United States (USA), 2003.
[23] J.J. Lienkaemper, D.P. Schwartz, K.I. Kelson, W.R. Lettis, G.D. Simpson, J.R. Southon, J.A. Wanket and P.L. Williams, Timing of paleoearthquakes on the northern Hayward Fault; preliminary evidence in El Cenito, California. Open-File Report OF 99-0318, p. 34, U.S. Geological Survey, Reston, VA, United States (USA), 1999.
[24] J.J. Lienkaemper, P.L. Williams, Evidence for surface rupture in 1868 on the Hayward Fault in North Oakland and major rupturing in prehistoric earthquakes, Geophys. Res. Lett. 26 (13) (1999) 1549–1952.
[25] E. Yu, P. Segall, Slip in the 1868 Hayward earthquake from the analysis of historical triangulation data, J. Geophys. Res. 101 (7) (1996) 16101–16118.
[26] T.R. Toppozada, G. Borchardt, Re-evaluation of the 1836 "Hayward fault" and the 1838 San Andreas fault earthquakes, Bull. Seismol. Soc. Am. 88 (l) (1998) 140.
[27] J.J. Lienkaemper, J.S. Galehouse, R.W. Simpson, Long-term monitoring of creep rate along the Hayward Fault and evidence for a lasting creep response to 1989 Loma Prieta earthquake, Geophys. Res. Lett. 28 (11) (2001) 2265–2268.
[28] J.C. Savage, M. Lisowski, Inferred depth of creep on the Hayward Fault, Central California, J. Geophys. Res. 98 (Bl) (1993) 787.
[29] R. Bürgmann, D. Schmidt, R.M. Nadeau, M. d'Alessio, E. Fielding, D. Manaker, T.V. McEvilly, M.H. Murray, Earthquake potential along the northern Hayward fault, California, Science 289 (5482) (2000) 1178–1182.
[30] R.W. Simpson, J.J. Lienkaemper, J.S. Galehouse, Variations in creep rate along the Hayward Fault, California, interpreted as changes in depth of creep, Geophys. Res. Lett. 28 (11) (2001) 2269–2272.
[31] W. Thatcher, T.C. Hanks, Source parameters of Southern California Earthquakes, J. Geophys. Res. 78 (35) (1973) 8547–8576.
[32] R.E. Abercrombie, Earthquake source scaling relationships from −1 to 5 M_L, using seismograms recorded at 2.5-km depth, J. Geophys. Res. 100 (B12) (1995) 24015–24036.
[33] S.T. Tse, R. Dmowska, J.R. Rice, Stressing of locked patches along a creeping fault, Bull. Seismol. Soc. Am. 75 (3) (1985) 709–736.
[34] S. Toda, R.S. Stein, P.A. Reasenberg, J.H. Dieterich, Stress 49 transferred by the Mw=6.9 Kobe, Japan, shock: effect on aftershocks and 50 future earthquake probabilities, J. Geophys. Res. 103 (1998) 24543–24565.
[35] K.P. Furlong, D. Verdonck, Three-dimensional lithospheric kinematics in the Loma Prieta region, California; implications for the earthquake cycle. In: R.W. Simpson (Ed.), The Loma Prieta, California, earthquake of October 17, 1989; Tectonic Processes and Models, pp. F103-F131, U.S. Geological Survey Profes. Paper Report: P 1550-F, Reston, VA, USA, 1994.
[36] T. Parson, Post-1906 stress recovery of the San Andreas fault system calculated from three-dimensional FE analysis, J. Geophys. Res. 107 (B8) (2002), doi:10.1029/20015B001051.
[37] M.A. D'Alessio, D.A. Schmidt, I. Johanson, R. Bürgmann, Estimates of slip rates on Bay Area faults from space geodesy, Eos Trans. AGU Fall Meet. Suppl. 84 (46) (2003) (T12E-02).
[38] C.W. Jennings, Fault activity map of California and adjacent areas, Geologic Map of California, Department of Conservation Division of Mines and Geology, 1994.
[39] R. Malservisi, Numerical models of the dynamics of lithospheric deformation at complex plate boundaries, PhD Thesis, Pennsylvania State University, 2002.
[40] G. Ranalli, Rheology of the Earth, Chapman & Hall, London, UK, 1995, 413 pp.
[41] H.J. Melosh, A. Raefsky, A simple and efficient method for introducing faults into finite element computations, Bull. Seismol. Soc. Am. 71 (5) (1981) 1391–1400.